

Polymer ejection from strong spherical confinement

J. Piili¹ and R. P. Linna^{1,*}

¹*Department of Computer Science, Aalto University, P.O. Box 15400, FI-00076 Aalto, Finland*

We examine the ejection of an initially strongly confined flexible polymer from a spherical capsid through a nanoscale pore. We use molecular dynamics for unprecedentedly high initial monomer densities. We show that the time for an individual monomer to eject grows exponentially with the number of ejected monomers. By measurements of the force at the pore we show this dependence to be a consequence of the excess free energy of the polymer due to confinement growing exponentially with the number of monomers initially inside the capsid. We show that the pressure inside the capsid driving the ejection dominates the process that is characterized by the ejection time growing linearly with the lengths of different polymers. We show that the superlinear dependence obtained for polymers amenable to computer simulations results from a finite-size effect due to the final retraction of polymers' tails from capsids.

PACS numbers: 87.15.A-, 82.35.Lr, 82.37.-j

Processes involving macromolecules in confinements are studied intensely due to their significance in biology and potential technological and medical applications. An important class of such processes is the capsid ejection where a polymer is initially in a compact conformation inside a capsid and then ejects outside through a pore a few nanometers wide. By far the most important biological process of this class is the viral packaging in and ejection from bacteriophages [1–9]. The recent technological advancement in using engineered viral capsids for drug delivery [10] calls for a thorough understanding of both polymer packaging in and ejection from a capsid.

There is a wide gap between the conditions under which biopolymers eject from viral capsids found *in vivo* and those taken to prevail in computer simulations and theoretical analysis. In the bacteriophages the viral DNAs are packed to almost crystalline densities [3], realization of which is beyond most computer simulations. Computational investigations of some specific characteristics using close-to-realistic model polymers packed to high densities are typically done using some form of probabilistic Metropolis sampling, see *e.g.* [11]. Investigations using dynamically more realistic molecular dynamics (MD) based methods are typically not very conclusive with regard to general characterization of the polymer ejection and do not attempt to relate to the existing theoretical formulations.

In the present Letter we study ejection of a fully flexible polymer from a spherical capsid using a realistic MD based method. Due to the computationally effective implementation of the capsid geometry we are able to simulate the ejection dynamics starting from unprecedentedly high initial monomer densities. Accordingly, we can show how the polymer's excess energy due to confinement determines the ejection dynamics, which decidedly deviates from the predictions based on the blob picture widely used for characterization of confined polymers under semidilute conditions. In what follows, we first outline the understanding obtained from the blob picture. We then describe our simulation method after which the results are presented and analyzed. Lastly, we summarize and recap the main conclusions.

The evolution of the theoretical understanding of the ejection

of a fully flexible polymer from a capsid was initiated by an investigation using Monte Carlo simulations [1]. Assuming the excess energy due to confinement to be $\Delta F/k_B T \sim N_0/R_0^{1/\nu}$ a scaling prediction for the ejection time of the form $\tau \sim N_0 R_0^{1/\nu} = N_0(N_0/\rho_0)^{1/3\nu}$ was obtained, where N_0 is the degree of polymerization, R_0 the capsid radius, ρ_0 the initial monomer density in the capsid, and ν the Flory exponent. This scaling was confirmed by MC simulations. In a later work [7] the excess energy due to spherical confinement was taken to follow the scaling $\Delta F/k_B T \sim (R_0/R_G)^{3/(3\nu-1)} \sim N_0 \phi_0^{1/(3\nu-1)}$, where $\phi_0 = N_0 a^3/R_0^3$ is the initial monomer volume fraction and a is the monomer length. This scaling law, first introduced by Grosberg and Khokhlov [12], was shown to be correct for the spherically confined polymer at ϕ_0 where the blob scaling in the semidilute conditions is valid [13]. This led to the scaling relation $\tau \sim N_0^{1+\nu} \phi_0^{1/(1-3\nu)}$, again confirmed by MC simulations.

The unified framework [8] for polymer decompression processes presented a fairly complete view of the ejection process. Assuming uniform polymer conformation the excess confinement energy inside a spherical capsid was derived in the same form as in [12],

$$\Delta F/k_B T \approx \left(\frac{a}{R_0}\right)^{3/(3\nu-1)} N(t)^{3\nu/(3\nu-1)}, \quad (1)$$

where $N(t)$ is the number of monomers inside the capsid.

The resultant driving force $\sim k_B T/\xi(t)$ was taken to be exerted on the monomer residing at the pore. The overall dissipation takes place close to the pore, within the range of the correlation length $\xi(t)$, where there exists a velocity gradient of segments of the order $\sim a\dot{N}(t)/\xi(t)$. Accordingly, the dissipation term was evaluated as $T\dot{S}(t) = \eta[\dot{N}(t)/\xi(t)]^2 \xi(t)^3$. The excess confinement energy is dissipated at the rate $\Delta\dot{F}(t) = -T\dot{S}(t)$, from which the time evolution was obtained as

$$N(t) = N_0(1 + t/\tau_1)^\beta, \quad (2)$$

where the exponent $\beta = (1 - 3\nu)/[2(1 - \nu)]$ and the time constant $\tau_1 \simeq \tau_0 \phi_0^{(1+\nu)/(1-3\nu)} N_0$. $\tau_0 \simeq \eta a^3/(k_B T)$

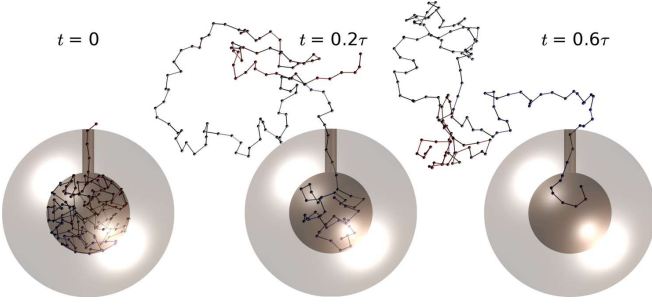


FIG. 1. (Color online) Snapshots of a simulated polymer ejection. (Images created using VMD [19] and POV-Ray [20])

is the monomer scale time constant, where η is the solution viscosity. For the pressure-driven part the scaling $\tau \sim \tau_0 \phi_0^{-(\nu+2)/(3\nu)} N_0^{(2+\nu)/(3\nu)}$ was obtained. [8]

For the simulation of the ejection dynamics we use a hybrid computational method where the time-integration of the polymer is performed by MD implemented by the velocity Verlet (vV) algorithm [14, 15]. The polymer is immersed in a solvent that is modeled by SRD [16, 17]. Here, we exclude the hydrodynamics for the better understanding of the fundamental ejection dynamics and more straightforward comparison with the existing understanding based on the blob picture. The spherical capsid is modeled as a shell with rigid walls imposing slip and no-slip boundary conditions for polymers and solvent, respectively. The pore is modeled as a cylindrical hole in the shell. The simulation geometry and snapshots of an ejecting polymer are depicted in Fig. 1. The pore radius R_p is 0.4 for the polymer and 0.8 for the solvent. The thickness of the capsid wall is 3. The capsid geometry was created using computationally effective constructive solid geometry technique [18].

The polymer is modeled as a chain of point-like beads with mass m_b . Adjacent beads are connected via the FENE potential $U_F = -\frac{K}{2} r_{\max}^2 \ln \left(1 - \left(\frac{r}{r_{\max}} \right)^2 \right)$, $r < r_{\max}$, where r is the distance between adjacent beads and K and r_{\max} are potential parameters describing the strength and maximum distance limit of adjacent beads. A Lennard-Jones potential acts between all beads: $U_{LJ} = 4.8\epsilon \left[\left(\frac{\sigma}{r_{ij}} \right)^{12} - \left(\frac{\sigma}{r_{ij}} \right)^6 \right] + 1.2\epsilon$ for $r_{ij} \leq \sqrt[6]{2}\sigma$ and $U_{LJ} = 0$ for $r_{ij} > \sqrt[6]{2}\sigma$. ϵ and σ are potential parameters and r_{ij} is the distance between beads i and j . The potential parameters are chosen as $\sigma = 1.0$, $\epsilon = 1.0$, $K = 30/\sigma^2$, and $r_{\max} = 1.5\sigma$ in reduced units [21].

We use initial monomer density $\rho_0 = N_0 / (\frac{4}{3}\pi R_0^3)$ instead of volume fraction ϕ_0 . Accordingly, the number of monomers N_0 corresponding to $\rho_0 = 1$ is by the factor $\frac{4}{3}\pi$ larger than N_0 corresponding to $\phi_0 = 1$. On the other hand, ϕ_0 was used for hard spheres, the use of which is not possible in high-density MD simulations. A value of ϕ_0 constitutes a slightly lower compression in a system using soft potentials than in one using hard-sphere potentials. This effect is more than compensated by our using ρ_0 instead of ϕ_0 , so effectively the systems

simulated here start from more compressed states than those dealt with in [1, 7, 8]. In the initial conformations four beads are inside the pore so the total length of the polymers is $N_0 + 4$.

SRD solvent consists of point-like particles whose dynamics can be divided into two steps. In the streaming step the solvent particle positions are ballistically propagated in discrete time steps. The interactions between particles are taken into account in the collision step. Here the random parts of the velocities for the polymer and solvent particles divided into cubic cells of unit edge lengths are rotated by the angle $\alpha = 3\pi/4$ around an axis chosen randomly for each cell. In the present case of Brownian heat bath velocities are randomly exchanged between all particles after the collision step. The solvent is kept at the constant temperature of $k_B T = 1.0$ by scaling the random parts of particle velocities such that the equipartition theorem holds at all times. In order to maintain Galilean invariance, the grid is shifted randomly at each time step [22]. For our simulations the vV time step $\delta t = 0.0002$ and the SRD time step $\Delta t = 0.5$. MD and SRD steps are performed in turns such that after $\Delta t / \delta t$ vV steps a single SRD step is performed. More detailed accounts of the SRD method can be found in [16, 17].

Fig. 2 (a) shows the ejection time τ vs number of monomers N_0 initially inside the capsid for different initial densities ρ_0 . In accordance with the previous findings [1–4, 6–9], scaling $\tau \sim N_0^\beta$ is obtained. Here, $\beta = 1.362 \pm 0.05$, 1.325 ± 0.04 , 1.293 ± 0.04 , 1.299 ± 0.03 , and 1.300 ± 0.04 for $\rho_0 = 0.5$, 0.75 , 1 , 1.25 , and 1.5 , respectively. β decreases slightly with increasing initial monomer density for $\rho_0 \leq 1$ in accordance with our previous findings [9] and statement on the case of driven translocation when the pore friction increases [23, 24]. Most of the effective friction ξ is exerted on the ejecting polymer in the vicinity of the pore through which the pressure pushes it. ξ increases with ρ_0 . As ξ increases $\tau \sim N_0^\beta$, $\beta \rightarrow 1$. In accordance with this reasoning, for polymers of $N_0 \geq 50$, $\tau \propto 1/\rho_0$ is obtained very precisely.

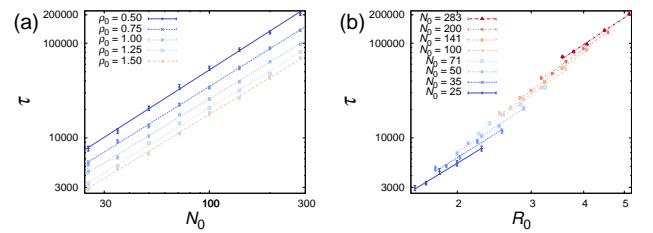


FIG. 2. (Color online) (a) Ejection time τ as a function of polymer length N_0 for different initial monomer densities ρ_0 . The points are averages over 40–50 runs. The lines are the fitted curves of the form $\tau \sim N_0^\beta$. $\beta = 1.362 \pm 0.05$, 1.325 ± 0.04 , 1.293 ± 0.04 , 1.299 ± 0.03 , and 1.300 ± 0.04 for $\rho_0 = 0.5$, 0.75 , 1 , 1.25 , and 1.5 , respectively. (b) τ as a function of capsid radius R_0 for different N_0 , $\tau \sim R_0^\zeta$. From bottom to top: $\zeta = 2.71$, 2.77 , 2.90 , 3.05 , 2.97 , 3.23 , 3.19 , and 2.92 for $N_0 = 25$, 35 , 50 , 71 , 100 , 141 , 200 , and 283 , respectively.

Fig. 2 (b) shows τ as a function of capsid radius R_0 . Com-

paring the obtained scaling $\tau \sim R_0^\zeta$, where $\zeta \in [2.71, 3.23]$, with the scaling in Fig. 3 (a) of [8], where ζ decreases from 5 toward 2 when R_0/a decreases from 10^2 toward 1, indicates that the ejection takes place in the very strongly confined regime. We also measured the radii of gyration R_g for the polymers' initial conformations inside the capsids. Spherical scaling $R_g \sim N_0^\theta$, where $\theta \approx 0.33$, was obtained for all ρ_0 , also confirming strong confinement. In spite of the strong confinement the ejected polymer segment remains close to equilibrium, since we measured $R_g(s) \sim s^{0.6}$ for the ejected segment at different stages. Magnitudes for $R_g(s)$ were also close to the equilibrium values.

Although ejection times τ scale with N_0 , as seen from the endpoints of the cumulative waiting times, $t(s)$ as such do not scale but grow exponentially with s , see Figs. 3 (a) and (b). Accordingly, waiting times of the ejecting monomers $t_w(s) = t(s) - t(s-1)$ follow the exponential form, $t_w \sim \exp(\kappa s)$, as seen in Fig. 3 (c), in accord with the waiting time profile found in [9] for the symmetric pore.

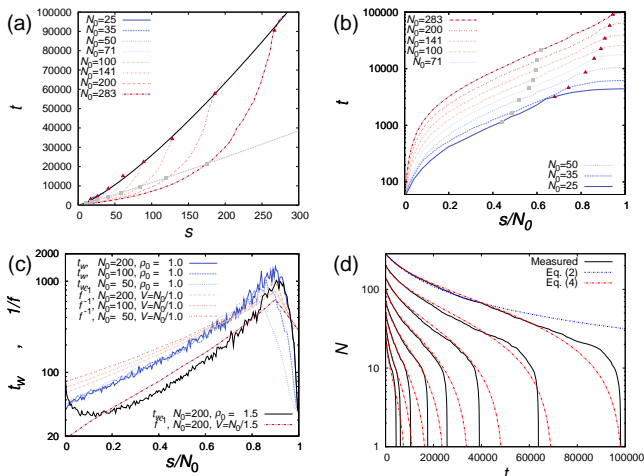


FIG. 3. (Color online) (a) The cumulative waiting time of simulations where $\rho_0 = 1.0$. Averages over 50 runs. The times when the end monomers of polymers of different lengths escape scale as $\tau \sim N_0^{1.29}$ (solid line). Reaction coordinates at instants when the inner part of the polymer exerts no force to the bead at the pore (\blacksquare): $s(\tau_2^*) \sim s^{1.0866}$ (dotted gray line). Reaction coordinate when number of beads inside the capsid $N = g_0$ (\blacktriangle) (b) The cumulative waiting time vs normalized reaction coordinate s/N_0 for $\rho_0 = 1.0$ and different N_0 . Squares (\blacksquare) and triangles (\blacktriangle) correspond to those in (a). (c) Waiting times t_w and the inverse of the measured force at the pore $1/f$ (arbitrary units) for $\rho_0 = 1.0$ and $N_0 = 50, 100$, and 200 ; and for $\rho_0 = 1.5$ and $N_0 = 200$. V is the capsid volume. (d) Number of beads in the capsid $N(t)$ during the ejection for the same N_0 as in (a) with fits to Eq (4) and the largest N_0 fitted to Eq. (2).

The form $t_w \sim \exp(\kappa s)$, or equivalently, $t_w(N(t)) \sim \exp(-\kappa N(t))$ is at odds with ΔF based on the blob picture, Eq. (1). To determine how largely ΔF determines $t_w(s)$ we measured the force f that has to be exerted on the monomer at the pore to keep it in position at different s . Fig. 3 (c) shows t_w and $1/f$ for $\rho_0 = 1.0$ and 1.5 . $1/f \sim t_w$ is seen to hold well for longer chains throughout the ejection until the start

of the final retraction of the remaining segment in the capsid. For $\rho_0 = 1.5$ this relation holds better, as is expected due to increased pressure driving the ejection. The initial deviation is caused by increased jamming at higher densities. Hence, ejection rate is dominantly determined by $\Delta F(N)$ at all stages except for the final retraction.

The exponential dependence $f = C \exp[BN(t)]$ arises due to excluded volume interactions: inside the capsid monomers interact individually rather than as ensembles of blobs and the higher order interaction terms become important. This observation is in contrast with the claimed screening of the excluded volume interactions at high concentrations giving rise to a different scaling than given by the semidilute blob picture, Eq. (1) [25].

Using the measured dependence $f = C \exp[BN(t)]$, we can derive $N(t)$ in the framework presented in [8]. If the monomers are packed inside the capsid by force applied at the pore, then the excess energy that results from packing N monomers is $\Delta F \approx \sum_{i=0}^{N-1} f_i \Delta l_i$, where f_i is the force required to move the bead i at the inner pore opening into the capsid and the bead $i+1$ in its place. Δl_i is the distance the bead $i+1$ needs to be moved. Since f_i is measured for individual beads, $\Delta l_i = a \approx 1, \forall i$. In the limit $\Delta l_i \rightarrow 0$ and the minimum necessary force being applied continuously on the polymer at the inner pore opening $\Delta F = \int_1^N f(n) dn = \int_1^N C \exp(Bn) dn = (C/B)[\exp(BN) - D]$, where B, C , and D are constants. $C \propto k_B T$ and from Fig. 3 (c) it is evident that $B = A/N_0$, where A is a constant. Relating the rate of change of this energy to the overall dissipation (see text after Eq. (1)), $\Delta \dot{F}(t) = -T \dot{S}(t) \approx \eta [a \dot{N}(t)/\xi(t)]^2 \xi(t)^3$, we get

$$\dot{N}(t) = -\frac{C}{\eta a^2 \xi(t)} e^{BN(t)}. \quad (3)$$

Approximating the correlation length to be constant $\xi(t) = \xi$ and using the initial condition $N(t=0) = N_0$, the solution is given in the form

$$N(t) = -\frac{N_0}{A} \ln \left(\frac{AC}{N_0 \eta a^2 \xi} t + e^{-A} \right). \quad (4)$$

Fig. 3 (d) shows the fit of Eq. (4) to the measured $N(t)$. A fit of $N(t)$ given by Eq. (2) for $N_0 = 283$ is given for reference. Eq. (4) is seen to describe $N(t)$ with excellent precision as it should given that $t_w \propto 1/f$ almost throughout the ejection.

For constant ρ_0 , the waiting times t_w as functions of the normalized coordinate s/N_0 fall on the same curve except for the final retraction, see Fig. 3 (c), so for this part $\tau \sim N_0$. The following calculation also confirms this: Figs. 3 (a) and (b) show the times τ_2^* when the measured force exerted by the polymer segment inside the capsid on a monomer at the pore is zero. These points, determined by measuring the force at the pore needed to keep segments of different lengths N completely inside the capsid, obey $N(t = \tau_2^*) = K N_0$, where $K \approx 0.38$. Solving Eq. (4) for $t = \tau_2^*$ gives

$$\tau_2^* = \frac{N_0 \eta a^2 \xi}{AC} (e^{-KA} - e^{-A}) = PN_0, P > 0 \quad (5)$$

for the pressure-driven part. This linear dependence does not result from $N(t = \tau_2^*) \sim N_0$ but is mainly due to ΔF not scaling with N , which can be shown by replacing ΔF of Eq. (1), by our measured exponential form in the framework presented in [8]. This leads to linear dependence for large N_0 .

From Fig. 3 (c) it is seen that $t_w(s/N_0)$ for different N_0 deviate from the common form only at the final stage of ejection when the remaining part of the polymer retracts from the capsid. Retraction speed increases identically for all polymers. After τ_2^* the force at the pore due to entropic imbalance between the outside and inside of the capsid causes the tension to propagate from the pore along the polymer segment in the capsid. The tensed segment Δs grows identically for all N_0 . Hence, $\Delta s/N_0$ will be larger for smaller N_0 resulting in retraction starting at smaller s/N_0 for shorter polymers, as seen in Fig. 3 (c). This finite-size effect results in superlinear scaling $\tau \sim N_0^\beta$, $\beta > 1$. Accordingly, for asymptotically long polymers linear dependence $\tau \sim N_0$ would be obtained.

In summary, we have investigated in detail the ejection of flexible polymers from spherical capsids through a nanoscale pore via computer simulations using realistic dynamics. The ejection dynamics and the pertaining excess energy due to confinement ΔF were analyzed via measured waiting time profiles and forces exerted on polymers at the pore. We found that the waiting times t_w grow exponentially with the number of ejected monomers and that the force f measured at the pore increases exponentially with the number of monomers in the capsid N . We showed that ΔF then must grow exponentially with N , which we addressed to be due to the higher-order terms in monomer-monomer interactions. We also found that $t_w \sim 1/f$ holds well for the simulated densities and that, accordingly, ΔF determines the ejection dynamics for such strongly confined polymers. We showed that this ΔF results in the ejection time τ growing linearly with the polymer length N_0 . The measured superlinear scaling $\tau \sim N_0^\beta$, $\beta > 1$, results from a finite-size effect related to tension propagation. Most importantly, already for densities that are moderate compared with realistic densities the strong monomer-monomer interactions result in the excess energy due to confinement increasing exponentially with the number of monomers in the capsid and ejection time increasing linearly on polymer length. This is in stark contrast with the previous results on ejection dynamics valid only in the semidilute regime. Equally important is

that for these densities the ejection is seen to easily complete without any assisting mechanism, such as flow.

We thank T. Sakaue for useful comments. The computational resources of CSC-IT Centre for Science, Finland, and Aalto Science-IT project are acknowledged. The work of Joonas Piili is supported by Tekniikan edistämissäätiö and The Emil Aaltonen Foundation.

* Corresponding author: riku.linna@aalto.fi

- [1] M. Muthukumar, Phys. Rev. Lett. **86**, 3188 (2001).
- [2] C. Forrey and M. Muthukumar, Biophys. J. **91**, 25 (2006).
- [3] D. E. Smith, S. B. Tans, S. Smith, S. B. Grimes, D. L. Andersen, and C. Bustamante, Nature **413**, 748 (2001).
- [4] P. Grayson, L. Han, T. Winther, and R. Phillips, Proc. Natl. Acad. Sci. U.S.A. **104**, 14652 (2007).
- [5] I. Ali, D. Marenduzzo, and J. M. Yeomans, Phys. Rev. Lett. **96**, 208102 (2006).
- [6] S. Ghosal, Phys. Rev. Lett. **109**, 248105 (2012).
- [7] A. Cacciuto and E. Luijten, Phys. Rev. Lett. **96**, 238104 (2006).
- [8] T. Sakaue and N. Yoshinaga, Phys. Rev. Lett. **102**, 148302 (2009).
- [9] R. P. Linna, J. E. Moisiö, P. M. Suhonen, and K. Kaski, Phys. Rev. E **89**, 052702 (2014).
- [10] J. Glasgow and D. Tullman-Ercek, Appl. Microbiol. Biotechnol. **98**, 5847 (2014).
- [11] D. Marenduzzo, C. Micheletti, E. Orlandini, and D. W. Sumners, Proceedings of the National Academy of Sciences **110**, 20081 (2013).
- [12] A. Y. Grosberg and A. R. Khokhlov, *Statistical Physics of Macromolecules* (American Institute of Physics, New York, 1994).
- [13] T. Sakaue and E. Raphaël, Macromolecules **39**, 2621 (2006).
- [14] W. C. Swope, H. C. Andersen, P. H. Berens, and K. R. Wilson, The Journal of Chemical Physics **76**, 637 (1982).
- [15] D. Frenkel and B. Smit, *Understanding molecular simulation: from algorithms to applications* (Academic Press, 2001).
- [16] A. Malevanets and R. Kapral, J. Chem. Phys. **110**, 8605 (1999).
- [17] A. Malevanets and R. Kapral, Novel Methods in Soft Matter Simulations **149**, 2258 (2004).
- [18] G. Wyvill and L. Kunii, T., The Visual Computer **1**, 3 (1985).
- [19] W. Humphrey, A. Dalke, and K. Schulten, Journal of Molecular Graphics **14**, 33 (1996).
- [20] Persistence of Vision Pty. Ltd., “Persistence of Vision (TM) Raytracer (Version 3.6),” (2004), [Computer software].
- [21] M. P. Allen and D. J. Tildesley, *Computer Simulation of Liquids* (Clarendon Press, Oxford, 2006).
- [22] T. Ihle and D. M. Kroll, Phys. Rev. E **63**, 020201 (2001).
- [23] V. V. Lehtola, R. P. Linna, and K. Kaski, EPL **85**, 58006 (2009).
- [24] V. V. Lehtola, R. P. Linna, and K. Kaski, Phys. Rev. E **78**, 061803 (2008).
- [25] A. Cacciuto and E. Luijten, Nano Letters **6**, 901 (2006).